5. K. L. Brown, “A second order magnetic optical achromat”, SLAC-PUB-2257 (1979).
6. A. Verdier, “Resonance free lattices for AG machines”, CERN-SL-99-018-AP, CERN-SL-99-18-AP (1999).
7. Y. Cai, K. Bane, R. Hettel, Y. Nosochkov, M.-H. Wang, M. Borland, “Ultimate storage ring based on fourth-order geometric achromats”, Phys.Rev.ST Accel. Beams 15 054002 (2012).
8. S. Fartoukh, “Achromatic telescopic squeezing scheme and its application to the LHC and its luminosity upgrade”, Phys. Rev. ST Accel. Beams 16, 111002 (2013).
9. Y. Cai, M. Donald, J. Irwin and Y. Yan, “LEGO: a modular accelerator design code”, SLAC-PUB-7642 (1997).
10. http://acc-physics.kek.jp/SAD/index.html.
11. B. Dalena, “Status of dynamic aperture and alignment for FCC-hh”, FCC Week 2017, Berlin, Germany (2017).
12. M. Giovannozzi, S. Fartoukh, R. De Maria, “Specification of a system of correctors for the triplets and separation dipoles of the LHC upgrade”, in Proc. IPAC 2013 Shanghai, China, WEPEA048 (2013).
13. S. Fartoukh, private communication.

2.21 Single-beam transverse collective effects for HE-LHC

David Amorim[#], Sergey Antipov[#], Sergey Arsenyev[#], Nicolo Biancacci[#], Xavier Buffat[#], Adrian Oeftiger[#], Lotta Mether*, Elias Métral[#], Tatiana Pieloni*, Benoit Salvant[#], Claudia Tambasco*, Frank Zimmermann#.

*Particle Accelerator Physics Laboratory, Institute of Physics, EPFL, Lausanne, Switzerland,
[#]CERN, CH-1211 Geneva 23, Switzerland

Mail to: Claudia.Tambasco@epfl.ch

2.21.1 Introduction

The High-Energy LHC (HE-LHC) aims at doubling the collision energy of beams circulating in the LHC tunnel thanks to the replacement of the current LHC magnets with magnets that can reach higher magnetic field [1].

This contribution describes the current status of studies on single beam collective effects in the transverse plane: space charge effects, transverse impedance and related beam stability and electron cloud effects. It is important to stress that this contribution is based on current assumptions and parameters, which may change significantly in the near future.

The list of parameters at the time of writing this contribution is in Table 1.

Table 1: List of HE-LHC parameters.

Parameter	Machine state	
	Injection	Flat top
Beam Energy [TeV]	1.3	13.5
Transverse Norm. Emittance [mm.mrad norm.]	2.5	
Bunch intensity [1E11]	2.2	
Bunch spacing [ns]	25	
RMS bunch length [m]	0.081	0.075
Betatron Tunes (Qx/Qy)	62.31/60.32	
RF Voltage V [MV]	16	30
Synchrotron tune Qs	1.19E-03	2.02E-03
RF harmonic number h_{RF}	35640	
Momentum Compaction Factor	3.23E-04	
Slippage factor	3.22E-04	

2.21.2 **Space Charge effects**

This subsection briefly discusses the relevance of typical detrimental and beneficial space charge effects for the LHC in the context of the higher-energy upgrade. Potentially detrimental effects include emittance growth inflicted by betatron resonances, dynamic aperture reduction due to tune modulation, and emittance growth due to transverse injection mismatch. On the beneficial side, the direct space charge tune *spread* significantly contributes to Landau damping of higher order single bunch head-tail modes at LHC injection (for the current and the High Luminosity upgrade impedance models). The following paragraphs will elaborate on these space charge effects.

Transverse space charge acts as a defocusing force. In comparison to the injectors, the self-fields of the beam inflict a relatively small negative tune shift on the particles traversing the beam distribution at the high energies of (HE-) LHC. For bunched beams in most synchrotrons, the longitudinal particle motion is much slower compared to the transverse plane. Therefore the transverse space charge detuning depends on the local line charge density in the bunch. For a 6D Gaussian distributed bunch, the maximum incoherent tune shift corresponds to the strong fields in the bunch centre. It amounts to [2]

$$\Delta Q_{x,y}(s) = -\frac{qN}{8\pi^2\varepsilon_0 m_p c^2 \gamma^3 \sqrt{2\pi}\sigma_s} \int \frac{\beta_{x,y}(s)}{\sigma_{x,y}(s)(\sigma_x(s)+\sigma_y(s))} ds \qquad (1)$$

where the transverse rms beam size reads (e.g. in x):

$$\sigma_x(s) = \sqrt{\frac{\beta_x(s)\varepsilon_x}{\gamma} + D_x(s)^2 {\delta_{rms}}^2} \qquad (2)$$

with q the charge per particle, m_p is the proton mass, ε_0 is the vacuum permittivity, N the bunch population, m_p the mass per particle, γ the Lorentz factor, σ_z the rms bunch length, $\varepsilon_{x,y}$ the normalised transverse emittances, δ_{rms} the rms dimensionless momentum deviation, $\beta_{x,y}(s)$ the betatron functions at position s along the ring and $D_x(s)$ the dispersion function. The relativistic speed factor β has been approximated with 1.

The space charge tune shift is largest at injection as it scales with the inverse energy squared, $\Delta Q_{x,y}^{SC} \alpha 1/\gamma^2$. Typical tune shift values are on the order of $\Delta Q_{x,y}^{SC} \alpha\ 10^{-3}$. Table 2 summarises some relevant values evaluating the machine integral in Eq. (1) for the HL-LHC v1.3 optics with fixed transverse emittances $\varepsilon_{x,y=}$ 2.5 mm.mrad. LHC refers to a bunch population of N=1.3 10^{11} and HL-LHC to N=2.3 10^{11}.

Table 2: Gaussian maximum space charge tune shift for different energies and bunch populations.

Machine	**Maximum Direct Space Charge Tune Shift**	
	Horizontal ΔQ_x^{SC} [10^{-3}]	**Vertical ΔQ_y^{SC} [10^{-3}]**
LHC at 0.45TeV	0.79	1.5
HL-LHC at 0.45TeV	1.7	3.2
HL-LHC at 0.9TeV	0.21	0.40
HL-LHC at 1.3TeV	0.070	0.13
LHC at 6.5TeV	3.8×10^{-4}	7.2e-4
HL-LHC at 13.5TeV	7.2×10^{-5}	1.4e-4

Since particles undergo synchrotron oscillations, they may sample different transverse self-field strength along the local bunch line charge density. In principle, incoherent tune modulation can increase the chaotic region in phase space and limit the dynamic aperture. Studies on the incoherent tune modulation due to the direct space charge forces with synchrotron motion found no significant impact for the LHC though [3]. For similar synchrotron tunes and equal or smaller space charge detunings in the higher-energy upgrade we do not expect this to change. The same study concludes that emittance growth due to transverse injection mismatch is not an issue for LHC. From current LHC operation and the extrapolation to smaller tune shifts for the HE upgrade, we conclude that betatron resonances are not expected to be a showstopper either.

For Gaussian distributed beams the self-fields are non-linear, thus the incoherent transverse tunes depend on the betatron amplitude. In absence of other detuning effects, the corresponding space charge tune spread reaches from the maximum tune shift to the bare machine tune. In the case of detuning with amplitude e.g. in the case of Landau octupoles, the incoherent tune shifts mix. Presently, the LHC is operated at a Landau octupole current of around 40A at injection, which leads to a tune shift on the order of $\Delta Q^{oct} \alpha\ 10^{-3}$ for particles at a betatron amplitude of about 1 rms beam size. Hence Landau octupoles and direct space charge provide detuning with amplitude of roughly the same

magnitude at LHC injection. Both tune spreads scale with $1/\gamma^2$.

The rigid head-tail mode 0 is unaffected by space charge as the beam self-fields move with the beam. In contrast, octupole magnetic fields as well as an active damper feedback system can suppress mode 0 instabilities, which is discussed later in this document. On the other hand, direct space charge affects the (higher-order) non-rigid head-tail modes: (i.) by depressing the mode frequencies due to the tune shift as well as (ii.) by potentially Landau damping instabilities due to the tune spread. Taking into account only the impedance model at HL-LHC injection (i.e. 450 GeV), the transverse mode coupling instability (TMCI) between mode 0 and mode -1 occurs above a threshold intensity of $N\alpha$ 6×10^{11}p/b. Studies including space charge have shown that the mode coupling is cancelled as a direct consequence of (i.) since mode -1 shifts away from mode 0 [4]. Furthermore, simulations for finite chromaticity show that, for HL-LHC beam parameters, space charge can effectively suppress a mode 1 head-tail instability. The instability is recovered when the emittance is increased twentyfold and hence space charge becomes too weak. The same mechanism might explain beam stability at LHC injection, where the mere impedance model including a resistive damper predict higher-order head-tail instabilities for positive chromaticities. These beneficial Landau damping effects of space charge could be lost at higher energies (specifically for increased injection energies) as space charge becomes less relevant: the real part of the coherent tune shift from the impedance decreases with $1/\gamma$ as opposed to $\Delta Q_{x,y}^{SC} \alpha 1/\gamma^2$. We recommend to investigate the contribution of space charge to Landau damping for the future injection energies for HE-LHC, as well as to study if lower Landau octupole current are needed at injection to allow for a larger dynamic aperture, since large octupole current is currently needed to fight electron cloud in the LHC.

2.21.3 **Beam impedance and stability scalings from FCC-hh and HL-LHC**

In this simple analysis we compare the transverse instability effects in the HE-LHC to the ones in the FCC-hh (hadron Future Circular Collider [5]) and the HL-LHC (High Luminosity LHC [6]). For the head-tail mode 0 (the "rigid bunch" mode) we consider two figures of merit: the coupled-bunch (CB) instability rise time in turns, and the ratio of the single-bunch (SB) TMCI threshold to the nominal bunch intensity:

$$n^{turns} \propto \frac{E\,\Delta s}{N_b \beta_{avg} \mathrm{Re}\{Z_T\}_{\mathrm{eff}}^{\mathrm{CB}}}$$

$$\frac{N_{th}^{TMCI}}{N_b} \propto \frac{\sqrt{E V_{\mathrm{RF}} h_{\mathrm{RF}}}\, l_b}{N_b C\, \mathrm{Im}\{Z_T\}_{\mathrm{eff}}^{\mathrm{SB}}}$$

Here E is the energy, Δs is the bunch spacing, β_{avg} is the average betatron function (smooth approximation), l_b is the full (4σ) bunch length, C is the circumference, $\{Z_T\}_{\mathrm{eff}}^{\mathrm{CB}}$ and $\{Z_T\}_{\mathrm{eff}}^{\mathrm{SB}}$ are the coupled-bunch and the single-bunch transverse effective impedances weighted with the local betatron functions (defined in agreement with the LHC Design Report [7]).

The absolute numbers for the figures of merit depend on yet undefined instability mitigation techniques. Therefore, in this chapter we only give a relative comparison

between the three colliders and assume no instability mitigation (zero chromaticity, no transverse feedback, and no Landau damping).

We assume that the coupled-bunch impedance is dominated by the low-frequency contribution of the beam screen at both injection and top energy (the contribution of the collimators is small due to the inductive by-pass effect). The most unstable coupled bunch mode samples the impedance at the lowest frequency line $f = (\mathrm{frac}[Q] - 1)f_{rev}$ giving an additional dependence on the circumference. Ignoring the inductive by-pass effect and the multi-layer composition of the beam screen wall, we arrive to a simple scaling law

$$\{Z_T\}_{\mathrm{eff}}^{\mathrm{CB}} \propto \frac{C^{3/2}\rho_{bs}^{1/2}}{b_{arc}^3}\frac{\beta_{arc}}{\beta_{avg}}$$

where ρ_{bs} is the resistivity of the beam screen wall, β_{arc} is the average betatron function in the arc, and b_{arc} is the aperture of the beamscreen in the most critical (vertical) plane. For the single-bunch impedance, the assumed scalings for the beam screen and for the collimators (resistive wall) are

$$\text{bs: } \{Z_T\}_{\mathrm{eff}}^{\mathrm{SB}} \propto \frac{C\rho_{bs}^{1/2} l_b^{1/2}}{b_{arc}^3}\frac{\beta_{arc}}{\beta_{avg}}$$

$$\text{coll: } \{Z_T\}_{\mathrm{eff}}^{\mathrm{SB}} \propto \begin{cases} \dfrac{L_{coll} l_b^{1/2}\rho_{coll}^{1/2}E^{3/2}}{\beta_{coll}^{1/2}\beta_{avg}\epsilon_N^{3/2}}, & \text{if the number of sigmas is the same} \\ \dfrac{\max(\beta_{arc})^{3/2} L_{coll} l_b^{1/2}\rho_{coll}^{1/2}}{\beta_{coll}^{1/2}\beta_{avg} b_{arc}^3}, & \text{if gaps are chosen to protect the arc} \end{cases}$$

where L_{coll} and β_{coll} are the total length and the betatron function of the collimators and ϵ_N is the normalized beam transverse emittance.

We assume that at top energy the single-bunch impedance is dominated by the collimators, and that the collimator gaps are chosen to keep the number of sigmas the same. At injection the single-bunch impedance is assumed to be a sum of contributions of the beam screen and the collimators with the gaps given by a scaling law (providing the range of uncertainty). The relative importance of the beam screen and the collimators is chosen based on the absolute numbers for the FCC-hh: $\mathrm{Im}\{Z_T\}_{\mathrm{eff\,bs}}^{\mathrm{SB}} = 2.7\ M\Omega/m$, $\mathrm{Im}\{Z_T\}_{\mathrm{eff\,coll}}^{\mathrm{SB}} = 0.8\ M\Omega/m$ (molybdenum-graphite collimator jaws with pure molybdenum coating are assumed). The unknown contributions to the impedance (pumping holes, BPMs, etc.) are assumed to scale together with the known contributions.

In the tables below we separate the somewhat uncertain impedances from the relatively well-defined abilities to damp the impedance effects (the columns "n^{turns} for same Z_T" and "N_{th}^{TMCI}/N_b for same Z_T"). The two numbers are combined in the columns n^{turns} and N_{th}^{TMCI}/N_b. For the estimates the injection energy of the FCC-hh is assumed to be 3.3TeV. The HE-LHC beamscreen is assumed to be of the FCC type in this paragraph. The lengths and the resistivities of the collimator jaws are the same in all three colliders, and the betatron functions in the collimators are the same in the HL-LHC and the HE-LHC and 5.6 times higher in the FCC-hh. The HE-LHC normalized emittance is $2.5\mu m$, the nominal bunch intensity is 2.2×10^{11}, the 4σ bunch length is $1.24\ ns$ in case of 0.45 TeV injection and $1.5\ ns$ in all other cases, the RF voltage is $14\ MV$ at injection and $32\ MV$ at top energy.

Table 3: Comparison at injection: $E_{HL-LHC} = 0.45$ TeV

	Coupled-bunch			Single-bunch		
	n^{turns} for same Z_T	$\{Z_T\}_{\text{eff}}^{\text{CB}}$	n^{turns}	N_{th}^{TMCI}/N_b for same Z_T	$\{Z_T\}_{\text{eff}}^{\text{SB}}$	N_{th}^{TMCI}/N_b
HE-LHC compared to FCC-hh	10 times worse	6.8 times better	1.5 times worse	2.5 times worse	1.4 - 3.7 times better	1.8 times worse – 1.5 times better
HE-LHC compared to HL-LHC	1.3 times worse	4.6 times worse	5.8 times worse	1.8 times better	1.8-3.7 times worse	1.0 - 2.1 times worse

Table 4: Comparison at injection: $E_{HL-LHC} = 0.9$ TeV

	Coupled-bunch			Single-bunch		
	n^{turns} for same Z_T	$\{Z_T\}_{\text{eff}}^{\text{CB}}$	n^{turns}	N_{th}^{TMCI}/N_b for same Z_T	$\{Z_T\}_{\text{eff}}^{\text{SB}}$	N_{th}^{TMCI}/N_b
HE-LHC compared to FCC-hh	5.0 times worse	6.8 times better	1.3 times better	1.4 times worse	1.3 - 2.6 times better	1.2 times worse – 1.8 times better
HE-LHC compared to HL-LHC	1.6 times better	4.6 times worse	2.9 times worse	3.0 times better	3.3 - 4.0 times worse	1.1 - 1.3 times worse

Table 5: Comparison at injection: $E_{HL-LHC} = 1.3$ TeV

	Coupled-bunch			Single-bunch		
	n^{turns} for same Z_T	$\{Z_T\}_{\text{eff}}^{\text{CB}}$	n^{turns}	N_{th}^{TMCI}/N_b for same Z_T	$\{Z_T\}_{\text{eff}}^{\text{SB}}$	N_{th}^{TMCI}/N_b
HE-LHC compared to FCC-hh	3.5 times worse	6.8 times better	1.9 times better	1.2 times worse	1.3 - 2.1 times better	1.0 - 1.8 times better
HE-LHC compared to HL-LHC	2.3 times better	4.6 times worse	2.0 times worse	3.6 times better	4.0 - 4.7 times worse	1.1 - 1.3 times worse

Table 6: Comparison at top energy

	Coupled-bunch			Single-bunch		
	n^{turns} for same Z_T	$\{Z_T\}_{\text{eff}}^{\text{CB}}$	n^{turns}	N_{th}^{TMCI}/N_b for same Z_T	$\{Z_T\}_{\text{eff}}^{\text{SB}}$	N_{th}^{TMCI}/N_b
HE-LHC compared to FCC-hh	4.9 times worse	6.6 times better	1.3 times better	1.6 times worse	1.9 times better	1.2 times better
HE-LHC compared to HL-LHC	1.5 times better	3.7 times worse	2.5 times worse	2.7 times better	2.5 times worse	1.1 times better

Based on the relative comparison for n^{turns} and N_{th}^{TMCI}/N_b we can conclude that for all of the studied cases except the injection at 0.45TeV, both figures of merit in the HE-LHC are better than in at least one of the compared colliders (FCC-hh or HL-LHC). Achieving stability in the 0.45TeV case might require more aggressive mitigation techniques than the ones anticipated for either of the compared colliders. In the end, the decision should rely on the absolute numbers rather than the relative comparison (see the detailed study below).

2.21.4 **Impedance model**

A first version of the HE-LHC impedance was derived from the LHC and HL-LHC impedance models [8, 9]. In these two cases the main sources of impedance are the collimation system and the beam screen.

The impedance simulations were performed for four different cases. These cases include three different injection energies (450 GeV, 900 GeV and 1.3 TeV per beam) and the top energy case (13.5 TeV per beam). The HL-LHC optics for injection and top energy with 48cm squeeze were used to provide the different elements beta functions.

As the collimators are required to sit close to the beam to ensure a sufficient cleaning efficiency, they are one of the main impedance contributors. Their physical gaps in mm were scaled according to the beam energy considered, the reference emittance and the gap in number of collimation sigmas σ_{coll} as reported in Table 7 for the two main collimators families. The physical gaps h are computed as follow:

$$h = n\,\sigma_{coll} = n\sqrt{\frac{\varepsilon_n}{\gamma_{rel}}\left(\beta_x \cos^2\varphi + \beta_y \sin^2\varphi\right)}$$

where n is the number of collimation sigmas as reported in Table 2, ε_n is the reference normalized emittance, γ_{rel} is the Lorentz factor, $\beta_{x/y}$ are the Twiss beta function at the position of the collimator and φ is the angle of the collimator with respect to the horizontal plane. For the top energy case, a preliminary collimators parameters file was provided by the collimation study team [10]. In this case, the Twiss beta functions at the collimators are the ones from a preliminary version of the HE-LHC optics. Among all, the primary and secondary collimators are the main contributors to the impedance as their gaps are in the order of a few mm. For the simulations, they are assumed to be made of molybdenum-graphite coated with a 5 μm deposit of molybdenum [11].

Table 7: Reference emittance and collimators gaps in number of beam sigmas for the HE-LHC scenarios considered and the HL-LHC injection and top energy scenarios.

Machine	**HE-LHC**	**HE-LHC**	**HE-LHC**	**HE-LHC**	**HL-LHC**	**HL-LHC**
Machine state	Injection	Injection	Injection	Flat-top	Injection	Flat-top
Beam energy	450 GeV	900 GeV	1.3 TeV	13.5 TeV	450 GeV	7 TeV
Reference emittance	2.5 µm	2.5 µm	2.5 µm	2.5 µm	2.5 µm	2.5 µm
Primary collimators	5.0 σ	5.7 σ	5.7 σ	5.0 σ	6.7 σ	6.7 σ
Secondary collimators	6.0 σ	6.7 σ	6.7 σ	6.0 σ	7.9 σ	9.1 σ
Injection protection	7.3 σ	8.0 σ	8.0 σ	N/A	9.5 σ	N/A
Machine aperture	~ 8 σ	> 10.6 σ	> 10.6 σ	To be defined	12.6 σ	~ 10 σ

The impedance model was first computed with the LHC beam screen geometry. To account for the possible usage of the FCC-hh beam screen in HE-LHC, a factor four was applied on the resistive wall contribution of this element [12]. This factor four is an estimation taking into account the tighter mechanical aperture and the increased material resistivity. In the FCC-hh beam screen case, the increased resistivity would come from using a beam screen cooled to 50 K instead of a beam screen cooled to 20 K in the LHC/HL-LHC case.

The horizontal and vertical dipolar impedances are shown in Figure 1 for the 450 GeV injection case, in Figure 2 for the 1.3 TeV injection case and in Figure 3 for the 13.5 TeV top energy case. In these plots the orange curves correspond to the LHC beam screen case and the blue curves to the FCC-hh beam screen case. For frequencies below 100 MHz the beam screen contribution dominates and the effect of the beam screen type is stronger. Above this frequency the collimators contribution dominates and the beam screen type has a small impact at injection energy and no impact at top energy.

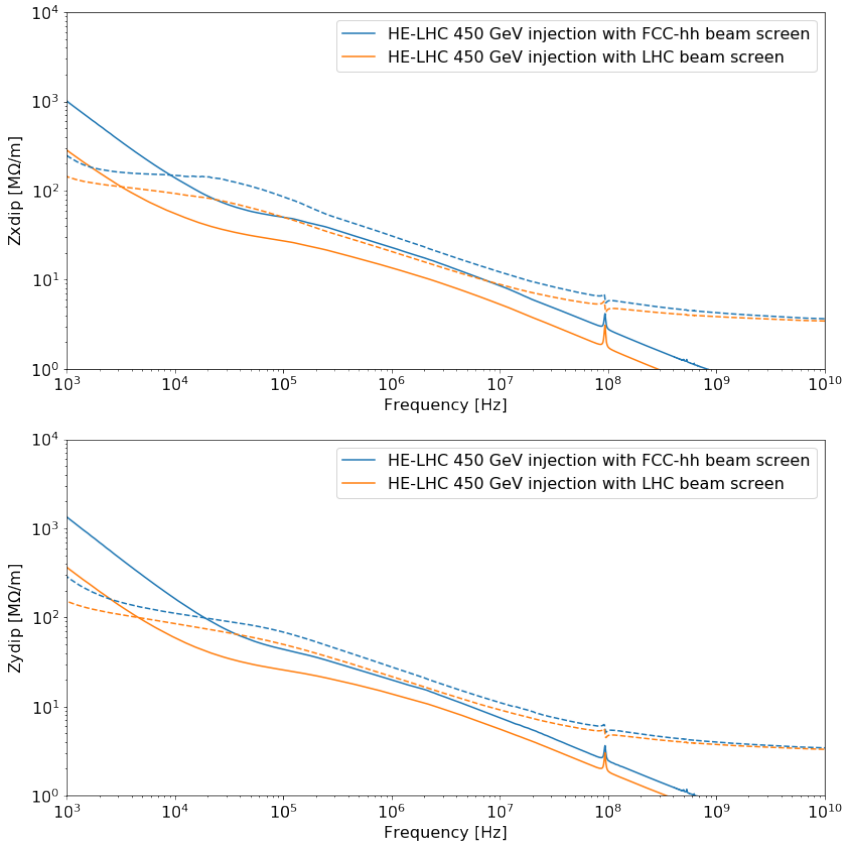

Figure 1: Transverse dipolar impedance at 450GeV injection energy. Solid line: real part. Dashed line: imaginary part.

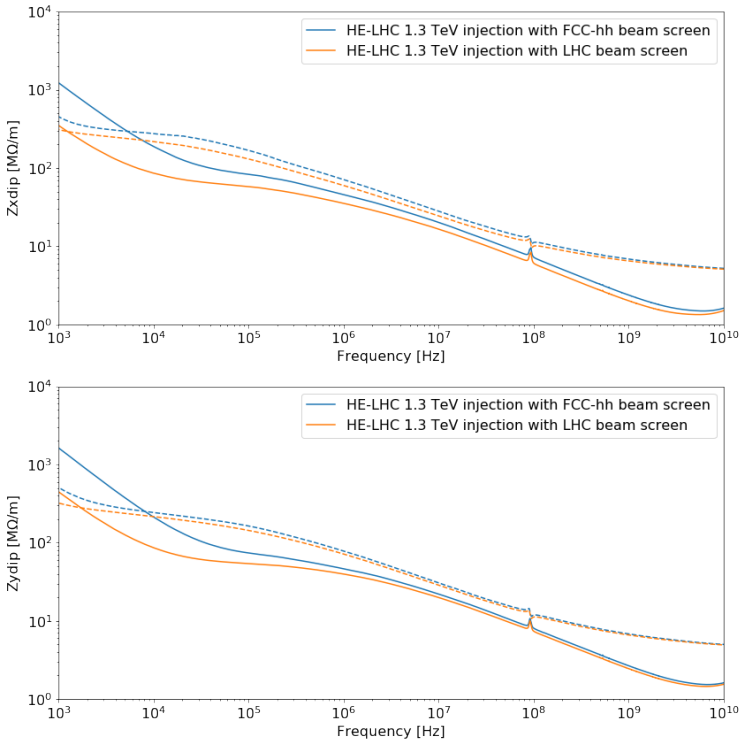

Figure 2: Transverse dipolar impedance at 1.3 TeV injection energy. Solid line: real part. Dashed line: imaginary part.

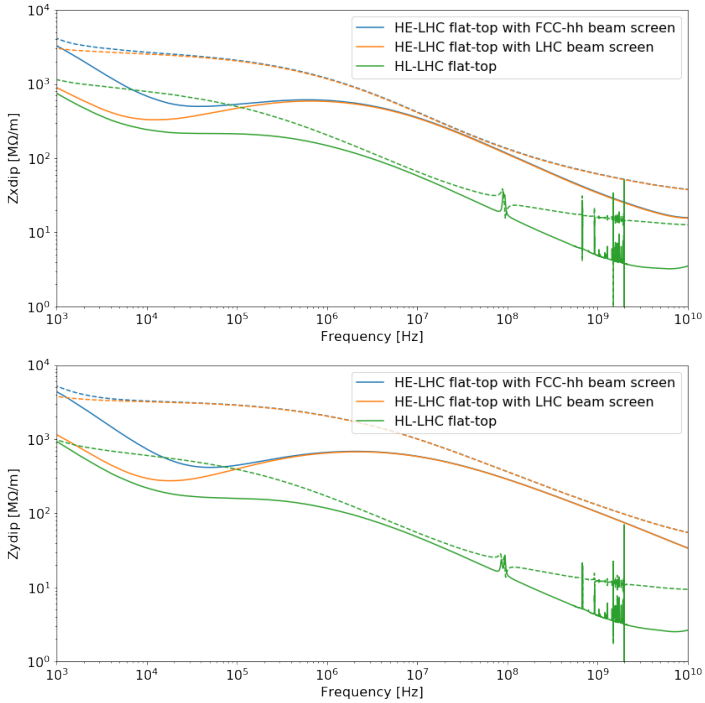

Figure 3: Transverse dipolar impedance at 13.5 TeV top energy. Solid line: real part. Dashed line: imaginary part.

For the top energy case shown in Figure 3, the green curve shows the HL-LHC impedance model for comparison. For frequencies above 100 MHz, a factor of 10 is present between the HL-LHC and the HE-LHC impedances due to tighter physical

collimator gaps. The HL-LHC impedance model also includes the crab cavities contribution as showed by a series of resonances in the GHz region. The crab cavities contributions were not taken into account for the HE-LHC impedance simulations.

2.21.5 **Elements contributions to impedance**

As seen previously the contributions of the beam screen and the collimators to the total impedance varies with frequency. Figure 4 and Figure 5 show the respective contributions of these elements for frequencies from 1 kHz to 10 GHz, for the 1.3TeV injection case and the 13.TeV top energy case. The collimator contribution is split between the geometric impedance (in blue) and the resistive wall impedance (in red). The beam screen contribution is split between the 50 K cooled sections of the beam screen covering 80% of the machine length (in pink) and the warm beam screen (in cyan).

For the 1.3 TeV injection energy case depicted in Figure 4, the real part of the beam screen impedance dominates for frequencies below 100 kHz. However, the imaginary part is dominated by the collimator impedance for all frequencies. The geometric contribution of the collimators dominates the imaginary part for high frequencies (above 1 GHz).

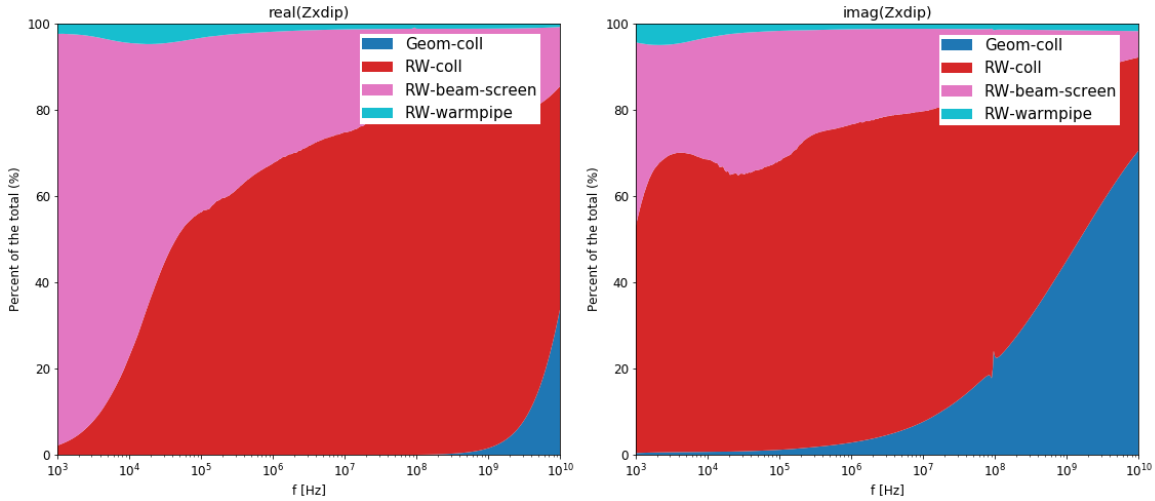

Figure 4: Transverse horizontal impedance contributions (in %) as a function of frequency for the 1.3 TeV injection case.

For the 13.5 TeV top energy case depicted in Figure 5, the distribution of the impedance follows the same behavior as in the injection energy case. However it can be noted that the resistive wall contribution of the collimators is even more important in this case.

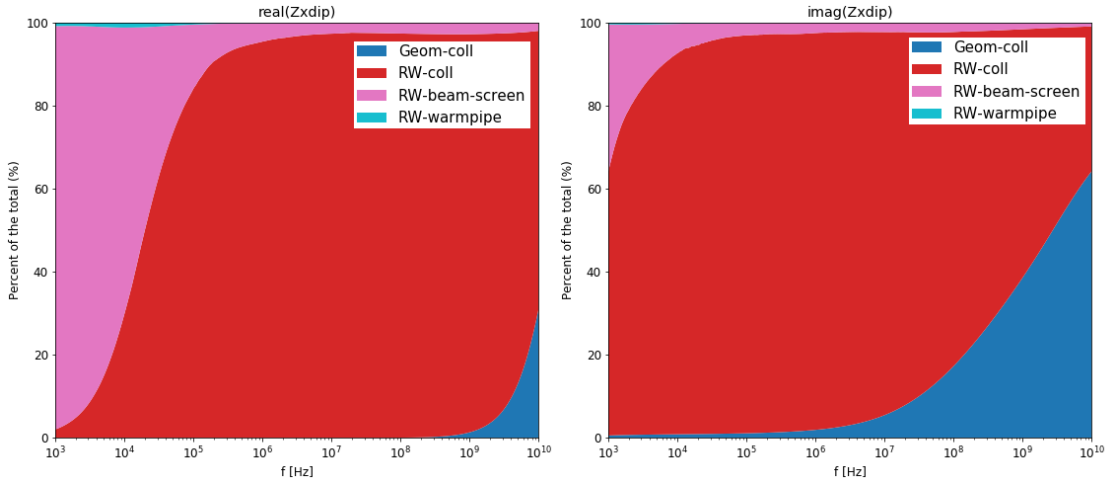

Figure 5: Transverse horizontal impedance contributions (in %) as a function of frequency for the 13.5 TeV top energy case.

We studied three scenarios of the injection energy: 450, 900, and 1300 GeV. The parameters of each scenario are summarized in Table 2. The advantage of the first scenario is that the injection energy can be provided by the current SPS, while the other two would require an upgrade of the injector. Its downside is the very tight aperture constraint at injection. It might be challenging if at all possible to ensure and maintain the hierarchy of the collimation and injection protection systems within the tight aperture constraints. The last option, 1300 GeV, seems preferable from the injection protection point of view and offers sufficient room to build the collimator hierarchy, but would require an expensive superconducting SPS and transfer lines.

From the impedance point of view, the injection energy of 1.3 TeV option is the most challenging one (Fig. 2). The increase of impedance with injection energy is caused by tightening of the collimator gaps, which follow the physical beam size and thus shrink as $E^{-1/2}$, with the E the energy. Compared to HL-LHC injection impedance of all studied options is higher due to smaller reference emittance.

However and similarly to the LHC and HL-LHC cases, the impedance budget of HE-LHC is higher at top energy because of the tighter collimators gaps required to ensure the beam cleaning efficiency. The collimators are the dominant contributor for a large range of frequencies. As the impedance budget is driving the coherent beam stability, alternative collimation systems could complement the present collimators. For example the use of an electron lens for halo collimation is proposed for HL-LHC [13] and could be used in HE-LHC as well.

2.21.6 **Beam stability and Landau damping**

The impedance driven modes may lead to coherent beam instabilities in hadron colliders, the Landau damping is a passive mechanism to stabilize the beam through the diversification of oscillations frequencies of the particles in the beams (tune spread). In order to be effective, the tune spread must overlap with the frequency of the unstable collective mode that has to be stabilized. At the LHC instability thresholds are evaluated by computation of the dispersion integral for a given detuning $\omega_{x,y}(J_x, J_y)$ and particle distribution $\psi(J_x, J_y)$ as a function of the transverse actions J_x and J_y in each plane [14]:

3
$$SD^{-1} = \frac{-1}{\Delta Q_{x,y}} = \int_0^{\infty} \frac{J_{x,y}}{\Omega - \omega_{x,y}(J_x, J_y)} \frac{d\psi}{dJ_{x,y}} dJ_x dJ_y \tag{3}$$

The solution of Eq. 3 provides the complex tune shifts at the stability limits for each frequency Ω defining the so-called stability diagram. Any non-linearities acting on the beams, such as beam-beam interactions, space charge and electron cloud, introduce a tune spread in the beams. At the LHC, Landau octupole magnets are used to provide enough tune spread to stabilize the beams by Landau damping mechanisms [15]. In particular, a linear detuning from octupoles magnets has been considered in the following analysis in order to evaluate the single beam stability by using the PySSD code [16] for HE-LHC.

The linear detuning from the octupoles magnets has been computed as [18]:

4
$$\begin{aligned} \Delta Q_x &= a \times I_x \varepsilon + b \times I_y \varepsilon \\ \Delta Q_y &= b \times I_x \varepsilon + a \times I_y \varepsilon \end{aligned}, \tag{4}$$

where I_x and I_y are the transverse actions normalized to the physical beam emittance and the coefficients a and b are defined as:

5
$$\begin{aligned} a &= 3.28 I_{oct}[\mathrm{A}] \times \varepsilon_n[\mathrm{m}] / E^2_{beam}[\mathrm{TeV}^2] \\ b &= -2.32 I_{oct}[\mathrm{A}] \times \varepsilon_n[\mathrm{m}] / E^2_{beam}[\mathrm{TeV}^2] \end{aligned} \tag{5}$$

where the LHC octupoles type has been considered for the evaluation of the coefficients a and b. The stability threshold is quantified in terms of the octupole current in the present LHC Landau octupole system, consisting in 168 octupoles, arranged in two families [15].

2.21.6.1 *Injection energy*

We studied three scenarios of the injection energy: 450, 900, and 1300 GeV. The last option, 1300 GeV, seems preferable from the injection protection point of view and offers sufficient room to build the collimator hierarchy, but would require an expensive superconducting SPS and transfer lines.

From the impedance point of view, the 1.3 TeV option is the most challenging one (Fig. 6). The increase of impedance with injection energy is caused by tightening of the collimator gaps, which follow the physical beam size and thus shrink as $E^{-1/2}$. Compared to HL-LHC injection impedance of all studied options is higher due to tight collimation settings.

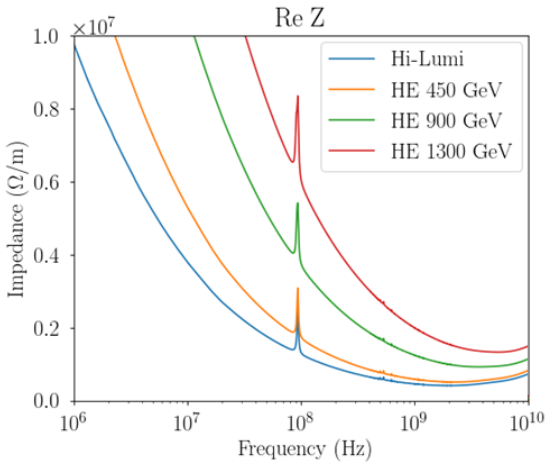

Figure 6: Impedance of HE-LHC at injection exceeds that of HL-LHC for all scenarios. The 1.3 TeV option is the most critical from the impedance point of view.

The tune footprints at injection energy E = 1.3 TeV for 6σ particles are shown in Fig. 7 for positive (red line) and negative (blue line) octupole polarity powered with the maximum achievable current of ±550 A. The footprints were computed by using the COMBI code [16]. In this configuration a maximum tune spread of $\Delta Q_{x,y} \approx 0.085$ both in horizontal and vertical plane is achieved.

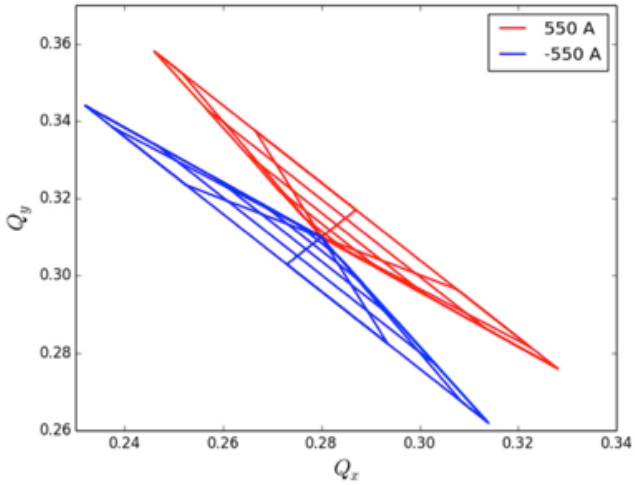

Figure 7: Tune footprint at 1.3 TeV injection energy for positive (red line) and negative (blue line) octupole polarity.

We have studied the coupled-bunch beam stability in the presence of the transverse feedback, chromaticity, and Landau octupoles using the NHT [19], DELPHI [20], and BIM-BIM [18] numerical solvers. The wakefields for NHT and BIM-BIM were extrapolated from the impedance model under the assumptions described before (see Sec. 1.1.4). The codes agree in their estimates, and in this Section we will present the results interchangeably. Since the lattice of HE-LHC is still under discussion, for the purpose of this study we assumed HL-LHC tunes and optics functions [21]; the key parameters for these studies are summarized in Table 8. The stability is quantified in

terms of growth rate of the most critical unstable mode and the amount of stabilizing octupole current required to suppress that mode. For the octupole threshold we assume the same stability diagram as in HL-LHC with negative polarity of the octupoles, quasi-parabolic transverse and normal longitudinal beam distribution, and zero coupling between the two transverse planes.

Table 8: Main beam and optics parameters

Machine state	***Injection***	***Flat-top***
Beam energy	450, 900, 1300 GeV	13.5 TeV
Tunes: x, y, s	0.31, 0.32, 0.005	0.31, 0.32, 0.002
Norm. emittance, rms	2 μm	2 μm
Bunch length, rms	9 cm	9 cm

NHT uses a unit convention, where mode frequency shifts $\mathrm{Im}\,\Delta\omega$ and damper gain g are normalized by the synchrotron frequency ω_s:

$$\Gamma[turns^{-1}] = 2\pi Q_s \,\mathrm{Im}\,\Delta\omega / \omega_s, \qquad d[turns^{-1}] = 2\pi Q_s g. \tag{6}$$

Figure 8 presents the results of the numerical simulation for the three injection energies, nominal HE-LHC intensity and number of bunches, two types of beam screens: LHC- and FCC-type. With the current LHC beam screen the growth rates remain small in the range of chromaticities Q' = 5 – 20 and for a damper gain higher than 1/50 to 1/100 inverse turns for all three cases. For these chromaticity and damper settings the octupole currents required to stabilize the beam remain relatively low: Ioct < 10 A for all scenarios.

A damper gain of 1/50 turns^{-1} or more is required in order to keep the instability growth rates at the same level for a tighter FCC-type beam screen, due to its higher impedance at low frequencies (Sec. 1.1.4). The most challenging option seems to be the lowest injection energy, where a feedback as fast as 25 turns is required. Provided sufficient damper gain and chromaticity in the range of 5 – 20, the octupole current required to stabilize the beam is small Ioct < 10 A.

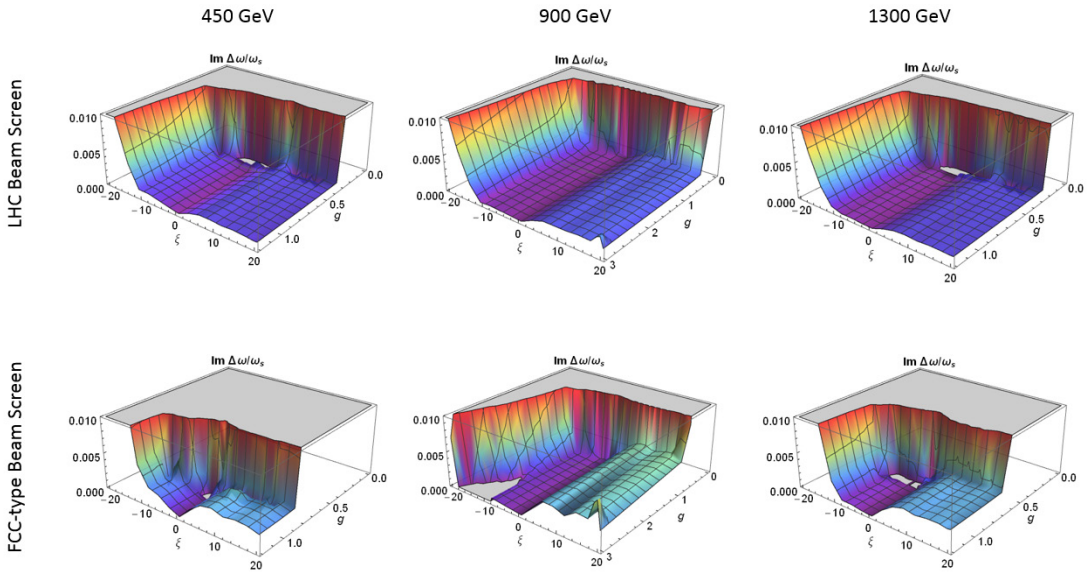

Figure 8: Growth rate of the most unstable couple-bunch mode for the LHC beam screen and FCC-type beam screen as a function of normalized gain (defined above) and chromaticity. 2748 bunches, 2.2×10^{11} ppb.

Apart from parameter scans for the nominal intensity, we also performed intensity scans to determine the safety margin with respect to couple-bunch TMCI and traditional head-tail instabilities. The mechanism and scaling estimates are discussed in detail in Sec. 1.1.3. We studied numerically the most critical case of Q' = 0 and several realistic damper gains. For a FCC-type beam screen there is no safety margin with a damper gain of 50 turns or below; a 25 turn gain is needed for a factor of two margin. The margin can be significantly improved with a bigger beam screen: for a LHC-type there is more than a factor of two margin for the nominal beam intensity (Fig. 9).

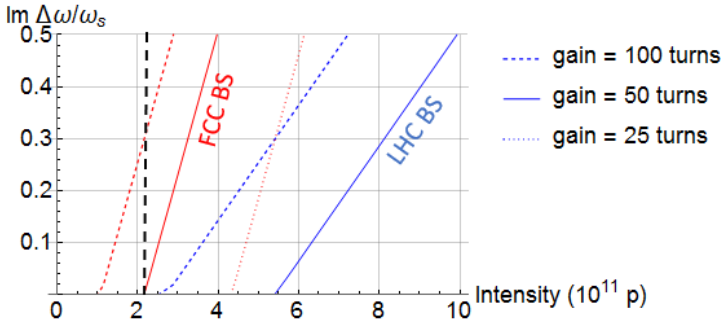

Figure 9: Stability thresholds as a function of damper gain. The safety margin in terms of beam intensity is small with a tighter beam screen and safe operation requires a higher damper gain. Growth rate for FCC beam screen are depicted in red, LHC – in blue; nominal intensity of 2.2×10^{11} ppb is shown by a black dashed line. E = 1.3 TeV, 2748 bunches, Q' = 0, no octupoles.

2.21.6.2 *Flat top energy*

The flat-top at 13.5 TeV is expected to be the most critical case from the machine impedance point of view. Since at the moment there is no solid baseline for HE-LHC collimator settings yet, we have assumed a collimator model similar to HL-LHC in order to create the impedance model. Based on the input from the collimation and machine protection [22] we put the primary collimators in IR-7 at 5 σ and the secondary – at 6 σ (Table 7). Note that these conservative estimates might be relaxed based on the outcome of machine protection studies.

Due to the increased beam rigidity at flat top energy (E = 13.5 TeV) the effectiveness of the octupole magnets is reduced. For a normalized beam emittance ε = 2.5 μm.rad, in order to achieve a similar amount of tune spread as in the LHC with design beam parameters (E = 7 TeV and normalized beam emittance ε = 3.75 μm-rad), an octupole current of 3080 A would be required considering the LHC octupole magnet technology and same averaged β-function at the octupoles. This can be easily evaluated rescaling linearly the octupole detuning with amplitude with respect to the LHC beam energy and emittance: $(\gamma^{\text{HE-LHC}}/\gamma^{\text{LHC}})^2 \times (\varepsilon^{\text{LHC}}/\varepsilon^{\text{HE-LHC}}) = 5.6$. With these assumptions, for HE-LHC collision energy, 940 Landau octupoles would provide the same amount of tune spread as in the LHC. This is shown in Fig. 10 where the LHC tune spread is represented by the black line and the HE-LHC footprint for 940 Landau octupoles is represented by the green line. As visible the tune spread expected for LHC is fully recovered. For completeness, the tune footprints for HE-LHC are also shown considering a current of ±550 A for positive (red line) and negative (blue line) octupole polarity.

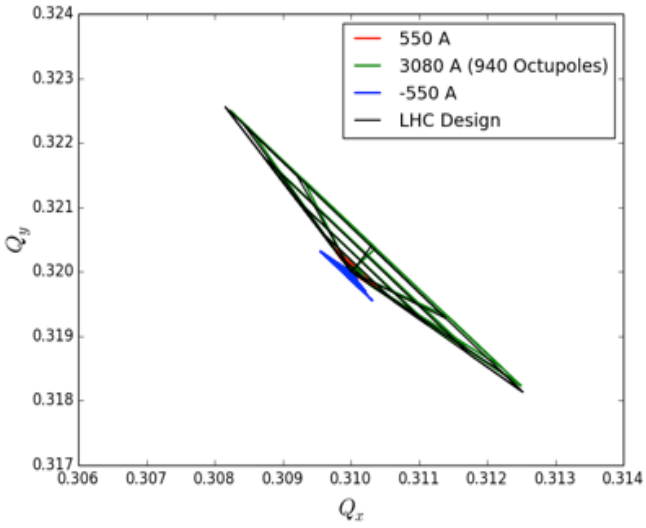

Figure 10: Tune footprints (till 6 σ particle) at flat top energy (normalized beam emittance ε=2.5 μm rad) for positive (red line) and negative (blue line) octupole polarity compared to LHC tune footprint with design parameters (black line). The green line represents the HE-LHC tune footprint for a current of 3080 A.

The impedance of the machine at 13.5 TeV flat-top is dominated by its collimator contributions (Sec. 1.1.4) and is not affected significantly by the choice of the beam screen at the frequencies relevant for single-bunch motion (Fig. 5). Due to tighter

collimator gaps, which scale with the beam size, the coupled-bunch instability growth rate might be rather large at the top energy (Fig. 11). Still the growth rate remains below 10^{-2} ω_s for Q' > 5 and damper gain higher than 100 turns. Even where the growth rate is relatively low, the octupole current required to stabilize the beam is large, since it increases as $1/\gamma^2$. It is estimated to reach at least 2000 A for 2 μm normalized emittance and Q' ~ 10 (Fig. 12), which is consistent with the current HL-LHC prediction of ~ 500 A where the top energy is 2 times lower (7 TeV).

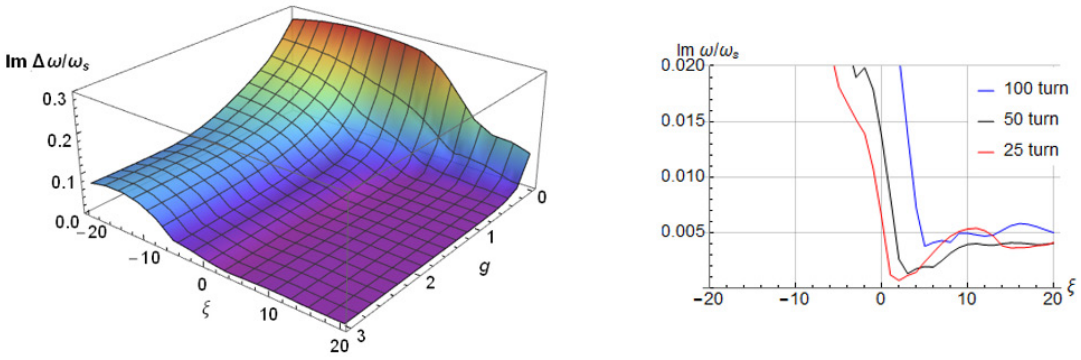

Figure 11: Growth rate of the most unstable coupled-bunch mode as a function of normalized gain and chromaticity. 13.5 TeV, 2748 bunches, 2.2×10^{11} ppb.

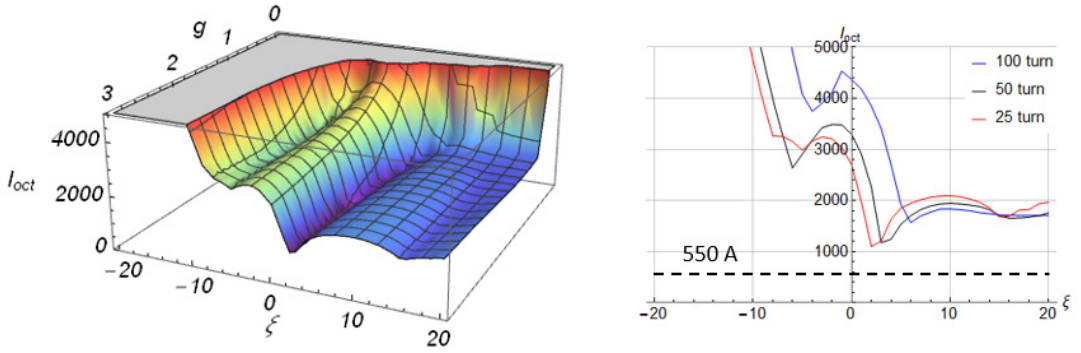

Figure 12: The octupole current required to stabilize the beam at flat-top exceeds the capabilities of the LHC octupoles. Left - octupole threshold as a function of normalized gain and chromaticity; right - cross-sections for several damper gains. The present octupole strength limit is shown by a black dashed line. 13.5 TeV, 2748 bunches, 2.2×10^{11} ppb, ε_n = 2.0 μm, negative octupole polarity.

From the past operational experience at LHC, a factor of two safety margin in the octupole current is recommended to ensure smooth operation. The amount of octupole current available at LHC – 550 A – is clearly insufficient for that purpose, lacking nearly an order of magnitude. Several options can be considered to tackle this problem: first, one can think of further reducing the machine impedance. Since the main contribution at flat-top comes from the collimator system, it is the primary candidate for improvement. The restive wall contribution of collimators could be further improved by utilizing novel low-resistivity coatings and the geometric part – by optimizing the collimator geometry. This

approach allows acting on both the real and the imaginary parts of impedance, thus lowering both the instability growth rate and the tune shift of unstable modes and reducing the octupole threshold.

Second, one might consider installing additional octupole magnets or upgrading the existing ones in order to increase their current. Figure 13 shows the stability diagrams obtained by the PySSD code [16] along with the most unstable single-bunch modes, computed using BIM-BIM [18] using the wake fields extrapolated from the impedance model under the assumptions described in Sec. 1.1.4. For positive chromaticity an octupole current of ~1875 A (~ 570 Landau octupole magnets) would be sufficient to damp the expected single bunch and multi bunch mode (Fig. 12), while a current of ~3281 A (~1000 Landau octupole magnets) is required to damp the expected single bunch mode for Q'~ -5 to -6. Considering the maximum achievable current of 720 A for the HL-LHC octupole magnet technology, the number of required octupole magnets can be reduced to 440 and 770 in the two cases, respectively. Compared to the number of octupoles in the LHC, the two cases correspond to an increase of the octupole magnets by factor of 2.62 and 4.58 respectively.

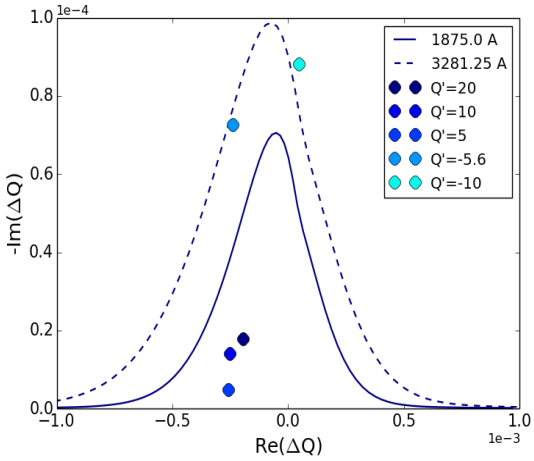

Figure 13: About 2000 A of octupole current is required to stabilize the beam at the top energy of 13.5 TeV. The most unstable single bunch modes were calculated by using the BIM-BIM code for different chromaticities. A normalized beam emittance of 2.0 μm.rad has been considered with a transverse feedback gain of 50 turns.

Another possible option is to optimize the machine focusing optics. For example, a telescopic optics can increase β-functions in the octupoles, increasing Landau damping. In the HL-LHC the telescopic squeeze increases the octupole footprint by a factor of two. This procedure might significantly reduce the number of additional octupole magnets required for HE-LHC. In order to fully benefit from it one will need to implement the squeeze during the energy ramp. This ramp-and-squeeze procedure may be technically challenging, and its feasibility and reliability has to be studied in detail.

Finally, more effective alternatives for Landau damping for high energetic hadron beams, such as electron lens [23] or RF Quadrupoles [24, 25] should be explored and discussed also in terms of the impact of such devices on dynamic aperture. Compared to octupoles, an electron lens offers a more efficient way to stabilize at high energies, because the tune spread it creates decreases only linearly with energy: $1/\gamma$ vs $1/\gamma^2$ for

octupoles. According to tracking simulations, in a real accelerator lattice the dynamical aperture improves if the octupole are replaced with an electron lens producing the same tune spread [23]. Since the spread is created by the core of the beam distribution, the electron lens stability diagram is also more robust than the octupole one, with depends on the population of the tails [26].

Electron lenses have been used in the past to create large tune spreads up to 10^{-2} and improve beam stability in Tevatron [27] and RHIC [28]. Preliminary estimates show that using an electron lens of existing HL-LHC design [13] (planned for halo cleaning), one can attain a tune spread of up to 5×10^{-3} with moderate electron currents (Table 9). The resulting stability diagram significantly exceeds the octupole one, allowing damping of all unstable couple-bunch modes at flat-top with a large safety margin (Fig. 14).

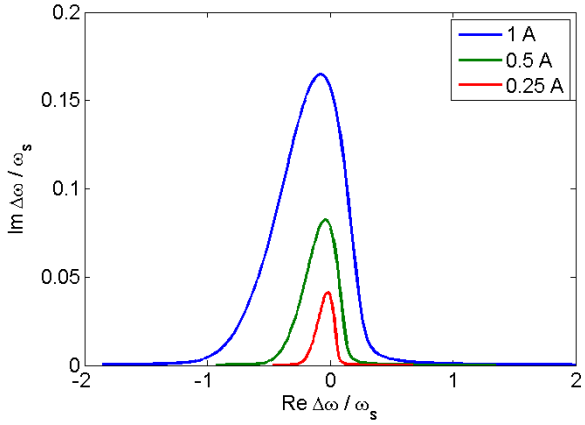

Figure 14: Stability diagrams for different currents in electron lens. E = 13.5 TeV, 2748 bunches, $2.2\text{x}10^{11}$ ppb, $\varepsilon_n = 2.0$ μm.

Table 9: Parameters of a Gaussian electron lens for Landau damping in the HE-LHC at the top energy

Parameter (Constraint)	*Value*	*Comment*
Current density	< 2-10 A/cm^2	Present technology limit
Electron current	< 1 A	HL-LHC E-Lens: up to 5 A
Electron beam length	3 m	
Electron energy	10 kV	
Max field ratio	B_m/B_g < 4.0 T/0.2 T = 20	HL-LHC E-Lens design
Electron beam size	0.4 – 2.0 mm	
Beta-function	240 m	40 m downstream IP-4
Proton beam energy	13.5 TeV	
Norm. emittance	2.0 μm	
Proton beam size	0.18 mm	
Transverse distribution	Gaussian	

2.21.6.3 *Electron Cloud effects*

The build-up of electron clouds may lead to coherent beam instabilities, through the interaction between the beam and the electrons. In order to assess the risk of electron

cloud induced instabilities, simulation studies identifying the conditions for electron cloud build-up have been performed.

2.21.6.4 *Effect of beam screen design*

The effect of two proposed beam screen options on electron cloud build-up has been studied in the arc dipoles with a field of 16 T. The beam screen designs that have been considered are an LHC-type beam screen with a saw-tooth structure in the impact area of the synchrotron radiation for reduced photon reflection [29] with the half apertures scaled to 14 and 19 mm in the vertical and horizontal plane respectively, and the FCC beam screen with ante-chambers for the synchrotron radiation and shielding of the pumping slots [30,31].

Photoelectrons produced by the impacting synchrotron radiation can play an important role in seeding the build-up, as is believed to be the case e.g. in the LHC [32]. Their effect could be even more important in the HE-LHC, where the number of synchrotron photons produced would be nearly double that of the current LHC, similar to the HL-LHC, and, due to the increased beam energy, a larger fraction of the photons would have an energy above the copper work function and could potentially produce photoelectrons.

In the HE-LHC dipoles, where the magnetic field lines confine the electron cloud build-up to vertical stripes around the beam, mainly photoelectrons produced at the top and bottom of the beam screen can contribute to the build-up. The transverse distributions of absorbed photons in the HE-LHC arcs have been estimated through simulations with the SynRad3D code [33] for the two beam screen options [34]. The amount of photons absorbed respectively on the top and bottom of the beam screen make up less than a percent of the total number of absorbed photons for both beam screen options, and for the FCC beam screen is roughly a factor of ten smaller than for the LHC type beam screen. The number of photoelectrons depends in addition on the photoelectron yield of the absorbed photons, which is not well known for the case in question. In the absence of an experimental estimate of the yield, the number of absorbed photons can be used as an upper limit for the number of photoelectrons.

Electron cloud build-up simulations have been set up with photoelectron seeding considering the results of the photon absorption studies to evaluate the effect of the beam screen design. Central electron densities as a function of the secondary electron yield (SEY) of the chamber surface have been estimated from the simulations, as shown in Figure 15. The threshold electron density for inducing single-bunch instabilities has been evaluated with analytical calculations [35] and beam dynamics simulations to around 10^{12} m^{-3} at flat top energy [36]. The electron density lies below the instability threshold at typical values of the SEY for both chamber options, however the FCC beam screen gives rise to a lower density, reflecting the smaller amount of photoelectron seeding. Also the heat load produced by the electron cloud, shown on the left in Figure 15, which has to be counteracted by the cryogenic system, is lower for the FCC beam screen, which is hence overall the more favourable beam screen option.

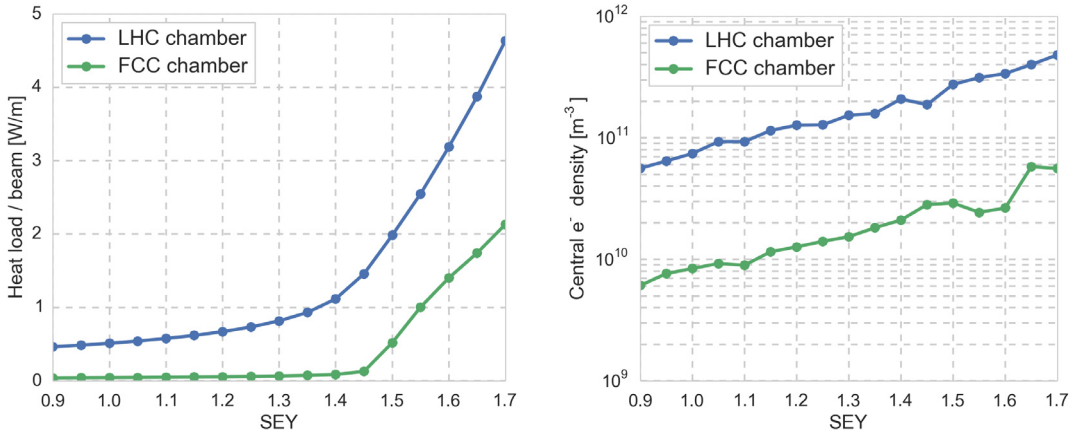

Figure 15: Comparison of the heat load and central electron density for the scaled LHC and the FCC beam screens for the nominal beam option.

2.21.6.5 *Effect of beam configuration*

Electron cloud build-up has been studied for the FCC beam screen in two main arc components: dipoles with a 16 T field and quadrupoles with a 220 T/m gradient, at injection (1.3 TeV) and at flat top energy. In addition to the nominal beam described in Table 1, two alternative beam options with the same total current as for the nominal beam have been considered: a beam with 12.5 ns bunch spacing, a bunch intensity of 1.1×10^{11} protons and normalized transverse emittances of 1.25×10^{-6} m, and a beam with 5 ns bunch spacing, bunch intensity 0.5×10^{11} and normalized transverse emittances of 0.5×10^{-6} m.

The estimated central densities for the three considered beam options at injection are displayed in Figure 16 for dipoles and quadrupoles respectively. The beam is more prone to instabilities at injection, where the threshold electron density for single-bunch instability has been estimated to around 10^{11} m^{-3} [36]. Taking into account that dipoles and quadrupoles cover around 80% and less than 10%, respectively, of the machine circumference, the nominal beam option could be prone to electron cloud induced instabilities if the SEY of the surface is above 1.4. Suppressing the electron cloud build-up with a low-SEY surface treatment, such as an amorphous carbon coating, would efficiently mitigate the occurrence of such instabilities. Also for the 12.5 ns beam option, electron densities above the threshold can be avoided by keeping the SEY at 1.1 or below. With the 5 ns beam option densities above the threshold can build up even for lower values of the SEY – this beam can be a viable option for the machine only with a surface treatment that guarantees a SEY no larger than unity.

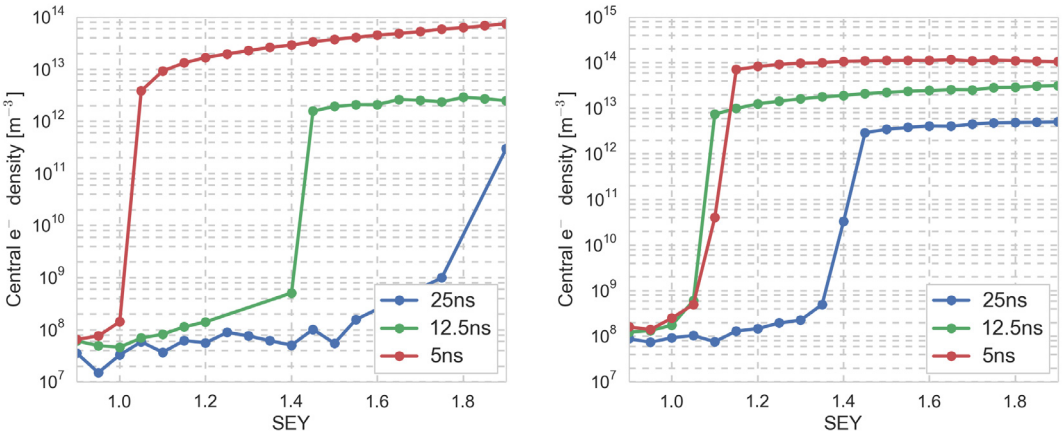

Figure 16: Central electron density as a function of SEY at injection energy for three different beam options in arc dipoles, on the left, and arc quadrupoles, on the right.

2.21.6.6 *Evolution during a fill*

Since electron cloud effects do not necessarily scale linearly with the bunch intensity, their evolution can change with the burn-off during a fill with luminosity production. This effect has been estimated with build-up studies, with decreasing bunch intensity and emittance. The central densities for the corresponding bunch intensities in dipoles and quadrupoles are shown in Figure 17. In dipoles only a mild dependence with intensity can be seen, whereas in the quadrupoles the multipacting threshold is seen to decrease and the central density increase with decreasing bunch intensity. In the absence of a surface treatment instabilities during fills could occur due to this effect, however a low-SEY surface treatment would be sufficient to prevent the build-up also for lower bunch intensities.

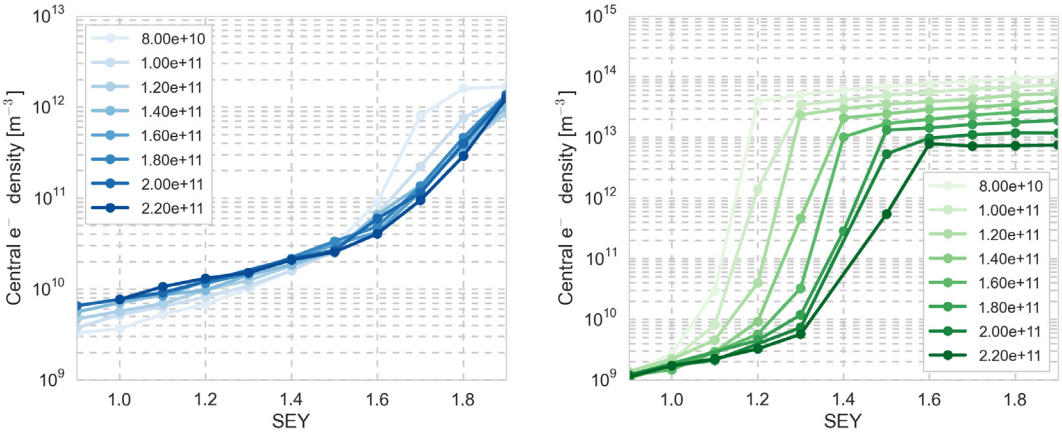

Figure 17: Central electron densities as a function of the SEY for the nominal beam with decreasing bunch intensity and emittance in arc dipoles, on the left, and arc quadrupoles, on the right.

2.21.7 Conclusion

Based on a set of preliminary parameters known at the time of writing this contribution, the impact of single beam transverse collective effects was addressed for HE-LHC and clear challenges identified in the design and baseline parameters have been identified: the instability thresholds are predicted to be low with an impedance model that accounts for the beam screens and the collimators and all available means to damp instabilities will need to be investigated to keep sufficient stability margin at both injection and flat top energies. A low SEY coating would be important to mitigate electron cloud related issues.

2.21.8 Acknowledgements

Work supported by the Swiss State Secretariat for Education Research and Innovation SERI.

We would like to thank the CERN collimation team for providing us with the collimator settings, in particular Roderik Bruce, Matthew Crouch and Stefano Pieloni.

2.21.9 References

1. E. Todesco, F. Zimmermann et al, “The High-Energy Large Hadron Collider”, proceedings of the 2010 EuCARD-AccNet-EuroLumi Workshop, Malta (2010).
2. F. Ruggiero, in Ch. 5, collective effects section, LHC Design Report, report CERN-2004-003-V-1 (2004).
3. F. Ruggiero and F. Zimmermann. "Consequences of the direct space charge effect for dynamic aperture and beam tail formation in the LHC." *Particle Accelerator Conference, 1999. Proceedings of the 1999*. Vol. 4. IEEE, 1999.
4. A. Oeftiger. “Single-Bunch Stability With Direct Space Charge.” *ICFA mini-workshop on Impedances and Beam Instabilities in Particle Accelerators*, Benevento, Italy (2017). Poster contribution, https://cds.cern.ch/record/2290575.
5. M. Benedikt et al, “FCC-hh Hadron Collider – Parameter Scenarios and Staging Options”, proceedings of IPAC 2015, Richmond, VA, USA (2015).
6. “High-Luminosity Large Hadron Collider (HL-LHC): Technical Design Report V. 0.1”, report CERN-2017-007-M (2017).
7. “LHC Design Report”, report CERN-2004-003-V-1, p. 98-100.
8. N. Mounet, “The LHC Transverse Coupled-Bunch Instability”, PhD thesis, Ecole Polytechnique, Lausanne (2012).
9. N. Biancacci et al., ”The HL-LHC Impedance Model and Aspects of Beam Stability”, proceedings of IPAC 2016, Busan, South Korea (2016).
10. M. Crouch, private communication, 11/10/2017
11. E. Quaranta et al., “Towards Optimum Material Choices for HL-LHC Collimator Upgrade”, proceedings of IPAC 2016, Busan, South Korea (2016).
12. S. Arsenyev and S. Antipov, “Impedance/stability/feedback consideration for FCC-hh and HE-LHC”, FCC-hh and HE LHC injector considerations meeting, CERN, Switzerland, 21/10/2017, https://indico.cern.ch/event/667297/ (2017).
13. G. Stancari, et al., Conceptual design of hollow electron lenses for beam halo control in the Large Hadron Collider, CERN-ACC-2014-0248 (2014).
14. S. Berg, F. Ruggiero,”Landau Damping with two-dimensional betatron tune spread", CERN, Geneva, Switzerland, CERN- SL (AP) 71, Dec. 1996.

15. J. Gareyte *et al.*, "Landau Damping, Dynamic Aperture and Octupoles in LHC", CERN, Geneva, Switzerland, LHC Project Report 91, Apr. 1997.
16. X. Buffat *et al.*, "Stability Diagrams of colliding beams", Phys. Rev. ST Accel. Beams 17 111002, 2014.
17. T. Pieloni, EPFL Thesis 4211 (2008).
18. X. Buffat, EPFL Thesis 6321 (2015).
19. A. Burov, Nested Head-Tail Vlasov Solver, Phys.Rev.ST Accel. Beams 17 (2014) 021007
20. N. Mounet. DELPHI: an analytic Vlasov solver for impedance-driven modes. HSC Meeting, CERN, Apr. 2014
21. R. Tomas, L. Medina, Parameter update for the nominal HL-LHC: Standard, BCMS, and 8b+4e, HL-LHC TC, CERN, Mar. 2017 (2017)
22. R. Bruce, M. Crouch, private communication
23. V. Shiltsev, et al., Landau Damping of Beam Instabilities by Electron Lenses, Phys.Rev.Lett. 119 (2017)
24. A. Grudiev, Radio frequency quadrupole for Landau damping in accelerators, Phys. Rev. Spec. Top. Accel. Beams 17 (2014).
25. M. Schenk *et al.*, "Analysis of transverse beam stabilization with radio frequency quadrupoles", PRSTAB 20, 104402 (2017).
26. N. Biancacci, E. Metral, C. Tambasco, Effect of tail cut and tail population on octupole stability threshold in the HL-LHC, HSC Meeting, CERN, Nov. 2015 (2015)
27. K. Bishofberger, Successful Beam-Beam Tuneshift Compensation, FERMILAB-THESIS-2005-105 (2005)
28. X. Gu, et al., Phys. Rev. Accel. Beams 20, 023501 (2017).
29. O. Brüning *et al.*, "LHC Design Report, Volume v.1: the LHC Main Ring", CERN-2004-003-V-1 (2004).
30. C. Garion, "FCC-hh beam screen studies and beam screen cooling scenarios," FCC Week 2016, Rome (2016).
31. I. Bellafont "Studies on the beam induced effects in the FCC-hh", EuroCirCol meeting, CERN, Oct. 2017 (2017).
32. P. Dijkstal *et al.*, "Simulation studies on the electron cloud build-up in the elements of the LHC Arcs at 6.5 TeV", CERN-ACC-NOTE-2017-0057 (2017).
33. G. Dugan, D. Sagan, "Synrad3D photon propagation and scattering simulations", Proc. Joint INFN-CERN-EuCARD-AccNet Workshop on Electron-Cloud Effects, La Biodola, Isola d'Elba, Italy, 5–9 June 2012, pp. 117–129, CERN-2013-002.
34. G. Guillermo *et al.*, "Simulating proton synchrotron radiation in the arcs of the HE-LHC", HE LHC design meeting 07, CERN, Nov. 2016 (2016).
35. K. Ohmi, F. Zimmermann, E. Perevedentsev, "Wake-field and fast head-tail instability caused by an electron cloud", Phys. Rev. E65, 016502 (2001)
36. K. Ohmi, "Electron cloud thresholds in HE-LHC", HE LHC design meeting 08, CERN, Dec. 2016 (2016).